NASA Technical Memorandum 103838

Documentation of Two- and Three-Dimensional Shock-Wave/ Turbulent-Boundary-Layer Interaction Flows at Mach 8.2

M. I. Kussoy and K. C. Horstman, Eloret Institute, Palo Alto, California

May 1991

National Aeronautics and
Space Administration

Ames Research Center
Moffett Field, California 94035-1000

NOMENCLATURE

M	Mach number
P	pressure
PT2	pitot pressure
PT2 INF	local free-stream pitot pressure ahead of interaction
P INF	local free-stream static pressure ahead of interaction
q,Q	heat flux
Q INF	heat flux ahead of interaction
Re	Reynolds number
RHO	density
RHO INF	local free-stream density ahead of interaction
RHOU	mass flux (ρu)
RHOU INF	local free-stream mass flux ahead of interaction
s, S	distance along fin surface measured from leading edge
T	temperature
T INF	local free-stream static temperature ahead of interaction
TT	stagnation temperature
TT INF	local free-stream temperature ahead of interaction
u, U	total velocity
U INF	local free-stream velocity ahead of interaction
x, X	streamwise coordinate, distance from leading edge of sharp fin or wedge
y, Y	distance normal to flat plate model surface
z, Z	spanwise distance measured from sharp fin surface

α	yaw or fin angle
δ	boundary-layer thickness
δ^*	compressible displacement thickness, $\int_o^\delta \left(1-\frac{\rho u}{\rho_e u_e}\right)dy$
θ	compressible momentum thickness, $\int_o^\delta \frac{\rho u}{\rho_e u_e}\left(1-\frac{u}{u_e}\right)dy$
δ	density
τ	shear stress

Subscripts

i	initial value
o	initial conditions
T	wind-tunnel stagnation conditions
w	wall
∞	local free-stream ahead of interaction

DOCUMENTATION OF TWO- AND THREE-DIMENSIONAL SHOCK-WAVE/TURBULENT-BOUNDARY-LAYER INTERACTION FLOWS AT MACH 8.2

M. I. Kussoy* and K. C. Horstman*

Ames Research Center

SUMMARY

Experimental data for a series of two-dimensional and three-dimensional shock-wave/turbulent-boundary-layer interaction flows at Mach 8.2 are presented. The test bodies, composed of simple geometric shapes fastened to a flat plate test bed, were designed to generate flows with varying degrees of pressure gradient, boundary-layer separation, and turning angle. The data include surface pressure and heat transfer distributions as well as limited mean flow field surveys both in the undisturbed and interaction regimes. The data are presented in a convenient form to be used to validate existing or future computational models of these hypersonic flows. Additional data are on a computer disk included with this document. This work was supported by a grant from NASA to Eloret Institute (NCC2-452).

INTRODUCTION

To design realistic aerodynamic vehicles to fly in the hypersonic flow regime, it is of primary importance to have the ability to predict, with reasonable reliability, the aerodynamic characteristics of such vehicles. Only in this manner can long and expensive design programs be significantly improved, and efficient designs identified and studied. However, before one attempts to predict the aerodynamics of the flow over a complex vehicle (with a cockpit, fuel tanks, and other appurtenant structures) flying at angle of attack, one should be able to reliably predict basic flow properties, such as surface pressures, heat transfer distributions, skin friction lines, extent of separation (if any), flow direction, etc. on simple generic shapes. Without verification of computations with experimental measurements on a simple body, any attempt at an a priori prediction of the flow field over a complex body would be an exercise in futility. The present authors have identified several key features of flows over such vehicles, and have designed test bodies composed of simple geometric shapes that give the above desired flow features.

Two configurations were tested; the first configuration consisted of a sharp wedge attached to a flat plate and the second a series of sharp fins attached to the flat plate (see fig. 1). Both the wedge and fin angles were varied, producing shock waves of various strengths. This resulted in both

*Eloret Institute, 3788 Fabian Way, Palo Alto, CA 94303.

attached and separated flow fields for the wedge flows, and complex three-dimensional (3-D) separated flow fields for the fin cases. Detailed boundary layer surveys have verified a fully developed hypersonic turbulent boundary layer on the flat plate alone.

The present paper presents experimental data obtained using these test models. The data obtained during this test program (undisturbed flow field surveys, surface pressure and heat transfer distributions, and several flow field surveys for two fin angles) can be used as a data base against which existing computer codes should be verified. In this way, turbulent flow models can be evaluated against relatively simple two-dimensional (2-D) and 3-D flows in which the basic flow characteristics of a more complex flow over a real vehicle are present.

The authors owe a large debt of gratitude to NASA Ames Research Center 3.5-Foot Hypersonic Wind Tunnel personnel, namely mechanical test technicians Mike Reeves (shift leader), Robert Finnie, and Reuben Torrecampo; and electronic technician Bong de la Cruz. Without their efforts during this investigation, the present results, obtained during a relatively short tunnel entry, would not have been possible.

DESCRIPTION OF EXPERIMENT

Facility

The experiment was conducted in the Ames 3.5-Foot Hypersonic Wind Tunnel where heated high-pressure air flows through a 1.067-m diameter test section to low pressure spheres. The tunnel is of the open jet design, which allows models to remain outside the stream until the required flow conditions are established. Models are then rapidly inserted, and just as rapidly retracted prior to tunnel shutdown. Damage to models and instrumentation are thus held to a minimum. The nominal free-stream test conditions were: total temperature = 1166 K, total pressure = 60 atm, free-stream unit Reynolds number = 5.× 10 /m and free-stream Mach number = 8.2. The test core diameter was approximately 0.6 m. Useful test time was 3 min. Run to run variations in pressure and Mach number were less than 0.5%. However the wind tunnel total temperature varied up to 50 K from run to run and, in addition, during a single run it varied about 50 K over the 3-min test time. These variations required special data reduction procedures which will be discussed later.

Test Bodies

Basic test bed– The test bed consisted of a sharp flat plate, 76 cm wide, 220 cm long, and 10 cm thick (see fig.1). The plate was pitched at –2° angle of attack to increase the test Reynolds number and provide a uniform two-dimensional flow field on the plate. The turbulent boundary layer thickness at the downstream end of the test bed was approximately 4 cm. The leading edge of the plate consisted of a 10° wedge. The bed was of a hollow frame construction, with interchangeable access panels (76 cm wide, 25.4 cm long, and 0.6 cm thick) covering the upper and lower surfaces. The entire test bed was watercooled, maintaining a constant surface temperature at 300 ± 5 K during a run. (Cooling was turned off during heat transfer runs.) There were 20-cm diameter holes in the

center of several of the interchangeable access panels for instrumentation, which would accommodate several different instrumentation ports. One port contained a series of pressure taps and two types of heat transfer instrumentation. Another port accommodated a computer controlled survey mechanism to which static pressure, total pressure, flow direction (yaw), and total temperature probes could be attached for flow field surveys.

Wedges– In the first series of tests a wedge was mounted above the test bed to generate a shock wave which impinges on the test bed (see fig. 1). Three wedges were tested, with angles of 5°, 10°, and 15°. These wedges were 76 cm wide, 61 cm long, and 5 cm thick at the rear, and were not instrumented. They were supported over the test bed by two thin plates (one on each side) which held the wedge so that its leading edge was 10.16 cm from the flat plate surface. The rear support plates had slots, which allowed the wedge to be rotated with respect to the flat plate. (A sketch of this arrangement is shown, see table 3.) So, for example, the 10° wedge was mounted over the flat plate with its upper surface parallel to the plate surface. With this configuration, the oncoming flow sees an inclined surface of 10° with respect to the flat plate surface. In subsequent runs, the wedge was pitched at an angle (while the wedge leading edge remains essentially 10 cm from the plate), so the inclined surface would make angles of 9°, 8°, 7°, etc. with respect to the oncoming flow.

To obtain continuous data throughout the interaction region, the wedge was also moved in the streamwise direction while the instrumentation port remain fixed. The undisturbed boundary-layer thickness at the incident shock-wave impingement point increased about 15% in a distance corresponding to the difference between the farthest upstream and downstream positioning of the wedge. However, this had little effect on the experimental results provided they were compared at an equivalent distance from the wedge leading edge.

Fins– In another series of tests, fins were placed on the test bed to generate a glancing shock-wave interaction and a three-dimensional mean flow. Fin angles of 5° to 15° were investigated using two basic models. One was triangular in shape (see fig. 1.), with an instrumentation port which could be replaced with a blank port for the flow visualization tests. This model had a slot machined in the rear, and could be pivoted around a point near the leading edge. In this manner, the angle the fin made with the oncoming flow could easily be varied from 5° to 15°, and this model was used to obtain all the fin surface data reported. Another fin design was used when obtaining the flow field data in the 3-D interaction regime. A sharp flat plate (2 cm thick) was used for this phase of the test program. Slotted "L" brackets were attached to the leeward surface, which allowed these fins (with fixed angles of 10° and 15°) to be translated in the Z direction and thus a variation of Z with respect to the fixed survey mechanism was obtained for each run. The fin leading edges were located on the flat plate 176 cm from the plate leading edge. They were all 30 cm long and 20 cm high.

Instrumentation

Two instrumentation ports were used in this investigation. Both of these ports (which were interchangeable with blank ports) had parallel rows of surface pressure taps, thermocouples, and heat transfer gauges installed in them. One port, rectangular in shape, was mounted on the fin surface, and the instrumentation rows ran in the Y direction. The other port, used on the test bed was 20 cm in diameter and had rows of parallel instrumentation which ran close to and on either side of the center

line. This port had a series of mounting holes along the edge, and could be oriented parallel (X direction), perpendicular (Z direction), or in any other direction with respect to the oncoming undisturbed flow.

Surface pressure– The surface static pressure taps were 0.16 cm in diameter, connected with short lengths of stainless steel tubing (10 to 15 cm long) to individual strain gauge differential-pressure transducers (PSI brand). These pressure cells were all located in a small self-contained modular unit, which had a built-in pressure scanning system (electrical, not mechanical). This system was designed to be calibrated in situ with carefully monitored pressures. These calibrations were made by varying the pressure on the reference side of the cell, and recording it using a Datametric strain gauge differential pressure cell which itself had been calibrated previously with a dead-weight tester. All calibrations were linear and repeatable to within 1%. All the transducers were located in a small module within the test bed and water cooled. The complex flow fields investigated herein usually encompass a wide pressure range. To obtain the highest accuracy, two pressure modules were used. One, to obtain accurate measurements of the free stream static pressure (of the order of 0.062 psia) as well as the other low static pressures present on the model surface and in the flow field had a range of ±1 psia. The other pressure modules had ranges of ±5 and ±45 psia.

Surface heat transfer– Surface heat transfer was obtained using two techniques—the transient thin-skin method, and a measurement using a thermopile. The transient thin-skin method utilized chromel-constantan thermocouples spot welded approximately 1 cm apart to the interior surface of the instrumentation ports. The port thickness was approximately 0.025 cm at that point. For these tests, the entire model was kept at room temperature, then inserted into the flow after the desired flow conditions were obtained. Depending on the thermocouple location, the temperature rise (with the internal model water cooling disconnected) varied from 10 to 50 K during a typical 20-sec heat-transfer run. The data were reduced by obtaining a least squares linear fit of $\ln [(T_T - T_w)/(T_T - T_{wi})]$ versus time. Calculations, using the procedures outlined in reference 1, indicated that for the present test conditions the interior wall temperature follows the exterior wall temperature after 2 sec and that longitudinal conduction errors are less than 5% of the measured convective heat transfer. Therefore these corrections were not applied to the data.

Heat transfer rates were also measured using miniature Schmidt-Boelter heat transfer gauges. These gauges, 0.20 cm diameter by 0.6 cm long, consisted of a thermophile to measure the temperature difference across a known substrate located just below the surface. An accurate factory calibration was used to relate the gauge output (in millivolts) to the heat transfer rate, Q. The calibration was linear. In fact, two calibrations were used, one with a range of Q from 0 to 3 BTU/ft_2 sec and the other with a range of 3 to 30 BTU/ft_2 sec, to obtain the highest measurement accuracy over the entire range of measurements. These gauges are essentially steady state devices, giving a reliable reading after about a second or two. They were placed 1 cm apart.

Parallel rows of thermocouples and Schmidt-Boelter gauges were placed in both the fin and flat plate instrumentation ports, and these data (along with surface pressures) were recorded simultaneously during a run.

The surface heat-transfer results were not corrected for the small longitudinal conduction errors (less than 5%) but were corrected for run-to-run variations in wind tunnel temperature. This was

done by assuming that the heat flux divided by the driving potential ($T_{Ti} - T_{wi}$) is invariant for small changes in total temperature. Therefore; q(corrected) = q(measured) $[(T_{Ti} - T_{wi_{nominal}})/(T_{Ti} - T_{wi_{nominal}}]$.

Survey mechanism– Flow field surveys were obtained with the computer-controlled survey mechanism located within the model. This mechanism was designed to move a probe in two directions—the vertical (Y) and in yaw, using individual motors. Precision anti-backlash gears were driven by stepping motors, whose shafts were capable of turning in controlled increments as small as 1.8/125°. The vertical motion was accomplished by a rack and pinion gear combination. The resolution of this mechanism in the vertical direction was 0.0003 cm. The resolution in yaw was 0.5°. The rotary motion of the motor shafts in both directions was coupled to anti-backlash bevel gears connected to multi-turn precision potentiometers.

Pitot pressure probe– Pitot pressures in the undisturbed flow field were measured by a stainless steel probe described in references 2 and 3. The probe was calibrated in a free-jet facility—matching Mach number, velocity and density with the present test conditions. This calibration indicated that the errors due to rarefaction effects was less than 1%; therefore no corrections were applied to the pitot data. This probe was attached to one port of the PSI module discussed above with a short length (about 8 cm) of stainless steel tubing. The pressure transducer calibration procedure was identical to the surface pressure procedure discussed previously.

Static pressure probe– Static pressures in the undisturbed flow field were measured by a stainless steel probe described in references 2 and 3. This probe is geometrically similar to the one used in reference 4, i.e., a 10 cone-cylinder. Independent calibrations to account for viscous interaction effects agreed with the calibration of Behrens (ref. 4). The viscous corrections applied to the data were up to 20%. The probe was attached to one port of the PSI module discussed above with a short length (about 8 cm) of stainless steel tubing. The pressure transducer calibration procedure was identical to the surface pressure procedure discussed previously.

Total temperature probe– Total temperatures in the undisturbed flow field were measured with the probe described in references 2 and 3. This probe was designed using a concept suggested by Vas' (ref. 5) An unshielded, butt-welded chromel-alumel thermocouple (0.3 cm long by 0.013 cm thick) is supported by tapered chromel and alumel posts. A second chromel-alumel thermocouple is formed at the end of the alumel support. This provides a simultaneous temperature measurement of the butt-welded thermocouple junction and the probe support.

Corrections for radiation, conduction and recovery factor were made following the method of reference 5. To make these corrections the local Mach number and Reynolds number must be known, requiring an iterative procedure using the pitot and static pressure data. Independent calibrations of these probes in the wind-tunnel free stream indicated a maximum total temperature error of 2%.

Cobra probe– In order to measure yaw angle and total pressure in the interacting flow field, a three hole flow direction probe (cobra probe) was used. The diameter of the individual probes was 0.107 cm, and the overall width was three times that, or 0.32 cm. The characteristics of this probe as well as some possible calibration techniques are discussed in reference 6. These probes can, within

limits recognized and defined from the calibration, be used in either of two basic modes. One mode is to simply null the probe, assuring that the pressures seen by the outer tubes are equal (taking into account the differing calibrations of the pressure transducers connected to each tube). Using this mode, a probe calibration (pressure vs. yaw for each tube) is only necessary to determine an "offset" due to minute physical asymmetries in fabrication. This procedure involves moving the probe to a Y location, waiting 3 or 4 sec for the outer tubes to give a steady reading, comparing these readings, determining which direction and how many degrees to rotate the probe, waiting again for a steady reading, comparing them again...etc. This is certainly "doable" using our high speed data acquisition system (Schwartz). But, with less than a 3 min run time available, a complete survey with respectable resolution in Y and yaw angle would probably take two or three separate tunnel runs.

Alternatively, we decided that a more practical method would be to calibrate the probe in the undisturbed boundary layer at several vertical positions, (thus varying Mach number) for a range of yaw angles. This would provide us with the zero offset, interference effects (when close to the model surface), as well as limitations in Mach number and maximum usable yaw angle range. The results of these calibrations showed that the probe calibration was independent of Mach number and thus usable for $Y > 0.2$ cm and ± 25 in yaw angle. With this technique the procedure was to fix the probe yaw angle and incrementally raise the probe through the boundary layer.

Experimental uncertainties– The uncertainties in the surface pressure were estimated to be $\pm 10\%$ or ± 80 N/m whichever is larger. The surface heat flux measurements were estimated to be $\pm 10\%$. For the flow field quantities, the estimated uncertainties are $\pm 2\%$ for the total temperature, $\pm 10\%$ for the static pressure, $\pm 6\%$ for the static temperature, $\pm 12\%$ for the density, $\pm 3\%$ for the velocity, ± 3 for yaw angle, and $\pm 5\%$ for the pitot pressure. The uncertainty in Y is ± 0.02cm. These uncertainties in the flow-field variables are due principally to zero offsets in the pressure and yaw angle measurements. Since each survey was obtained with a single probe, the uncertainty of the vertical variation in these flow-field quantities is significantly less than the numbers quoted above.

EXPERIMENTAL RESULTS

The test data were obtained during a series of runs with the wind tunnel operating at the nominal conditions described above. Before each run, the test body was positioned outside of the open jet. Flow was then initiated. When the desired test conditions were reached, the model was inserted into the test stream. The model was retracted prior to tunnel shutdown.

Undisturbed Test Bed Results

To establish the presence of a fully developed, equilibrium, hypersonic, turbulent boundary layer approaching the interaction region, pitot pressure, static pressure, and total temperature surveys of the boundary layer were taken at a distance of 187 cm from the flat plate leading edge. For these undisturbed boundary layer surveys, the flat plate test body was run devoid of any wedges or fin appendages. Natural transition from laminar to turbulent flow occurred between 50 and 100 cm from the leading edge. Velocity, density, and pressure profiles were obtained from the pitot and static

pressure and total temperature surveys. Each survey was taken during a single test run. In traversing the flow field, the probe was stopped at each location for a few seconds to ensure no time lag in the pressure or temperature measurement. Survey data were obtained up to 4.0 cm from the flat plate model surface. The static pressure at the model surface was monitored continuously during all traverses to verify that the data were free from interference effects. The data presented here have assumed a constant static pressure through the boundary layer. Actual measurements, after applying the viscous interaction correction, indicated a random variation of ±5%. Therefore a constant value was used. The velocity profiles obtained from these mean flow-field surveys were transformed into incompressible coordinates using the Van Driest II transformation (ref. 7) and are shown in figure 2 in law-of-the-wall coordinates. Also shown on this plot is Coles' universal law-of-the-wall (ref. 8). These profiles verify the presence of a hypersonic fully developed turbulent boundary layer in the interaction region for the wedge and fin flows being investigated. Using the law-of-the-wall concept, surface skin friction can be determined, and this value was $C = 0.98 \times 10^{-3}$. For any turbulence model verification procedure, these initial boundary layer conditions should be verified (or set) by the computation. The measured local free-stream conditions are given in table 1. Quantities measured during the surveys, as well as derived quantities, are presented in table 2 for the undisturbed boundary layer. For both the wedge and fin flows, the leading edge is forward of this location (X = 187 cm). Therefore a suitable boundary layer code should be used to extrapolate upstream for appropriate initial conditions.

The flat plate instrumentation port was aligned with its rows of instrumentation parallel to the flow direction and measurements were made with it from the most downstream to the most upstream position on the flat plate physically possible. The resulting longitudinal pressure and heat transfer distributions are shown in figures 3 and 4 respectively. Essentially a constant gradient of surface pressure is evident. The heat transfer decreases gradually from x = 100 cm. It is speculated that the end of natural transition occurred here although we have no direct measurements through the transition region.

The flat plate instrumentation port was also oriented perpendicular to the oncoming flow. These results indicated that both pressures and heat transfer rates were essentially constant over an 18-cm-wide, centrally located zone on the model surface both 165 and 190 cm back from the leading edge. (Variations in these data within this zone were within the experimental accuracy of the measurements.) Also, results from surface oil film studies showed a much wider area of surface skin friction lines parallel to the flat plate center line. From these results it was concluded that the flow was two-dimensional over the central model region being investigated.

Obviously we have a well behaved two-dimensional boundary layer over our flat plate test bed, running parallel to the plate edges (observed from oil flow visualization traces), with negligible longitudinal gradients, and becoming quite large (nearly 4 cm high) at the rearward stations where the interactive flows being investigated will be positioned.

Wedge Interaction Results

To measure the surface conditions over the entire wedge/ flat flate interaction region, including free-stream, peak values, and beyond, it was necessary to position the wedge in at least two locations

with respect to the stationary instrumentated flat plate port. In table 3 the range of wedge orientation (distance and angle) for each configuration is given. Because of the physical constraints of mounting holes, port location, etc., the shock from the wedge leading edge intersected the flat plate boundary layer significantly upstream of the station (X = 187 cm) where the undisturbed boundary layer surveys were done. Therefore, for these cases, a suitable boundary layer code should be used to extrapolate upstream for appropriate conditions.

The non-dimensionalized surface pressures and heat transfer results for wedge angles of 5°, 8°, 9°, 10°, and 11° are given in tables 4 and 5, respectively. In addition, these quantities, for angles of 5°, 8°, and 10° are shown in figures 5 and 6. From the oil flow visualization results it was apparent that the boundary layer for the 5° case was attached, for the 10° case it was separated, with the incipient separation occurring at 8°.

Fin Interaction Results

Oil flow visualization observations were made on both the flat plate and fin surfaces, using a thin mixture of machine oil and chalk dust. The oil would burn off or flow downstream, leaving a thin trace of chalk dust on the surface, which could be lifted off (using special wide scotch tape) and permanently placed on a plain white sheet. Surface flow angles could then be precisely measured. Angles measured on the flat plate surface using such a technique are given in table 6 and also drawn in figure 7 for the 10° and 15° fins. For both fin angles, both a primary and a secondary convergence line were observed. The primary separation lines were located at Z = 6.8 and 7.5 cm for 10° and 15° fins, respectively, at this streamwise location (X = 16.5 cm). The secondary separation lines were located at Z = 3.5 cm for both cases. Surface pressures and heat transfer rates were measured on both the fin surface and the adjacent flat plate surface for fin angles of 5°, 7.5°, 10°, 12.5°, and 15°. These results are given in tables 7, 8, 9, and 10 and also in figures 8 to 11.

Two sets of flow field surveys were done, one for the 10° and the other for the 15° fin. For the 10° fin, the axis of the cobra probe was set at 12° to the undisturbed flow. This angle was chosen as a compromise, based on flow angles in the free stream (0°), near the fin vertical surface (obviously 10°), and angles measured on the flat plate surface (obtained from the oil-flow visualization technique). It was felt that setting the probe at this angle would ensure that it would always be operating within its valid calibration range. A vertical survey was done in a manner similar to that described above for "single" probes. The flat fin was then translated in the Z direction a given distance (using the slot arrangement described above) and another survey run. For the 15° fin, the cobra probe was set at 18° to the flow, otherwise the survey method remained the same. The data obtained from these flow-field surveys, namely yaw angle and pitot pressures, are given in tables 11 and 12. These data are the results of averaging many data points at each Y location taken during each individual survey.

CONCLUDING REMARKS

Several cases of shock-wave/hypersonic, turbulent-boundary-layer interaction flows for both 2-D and 3-D geometries have been experimentally investigated. The resulting flows were

two-dimensional (with and without separation) and three-dimensional (with separation). These particular flows were chosen because they were relatively simple, but yet exhibited the same basic characteristics present on complex hypersonic vehicles.

Surface pressure and heat transfer distributions, as well as flow-field surveys (both in the undisturbed and interaction regime) are presented. The tabulated results presented in this report provide, in sufficient detail, experimental data for validating present or future turbulence models and computer codes. This validation procedure is necessary before attempts are made to compute more complex flows over realistic flight vehicles.

REFERENCES

1. George, A. R.; and Reinecke, W. G.: Conduction in Thin-Skinned Heat Transfer and Recovery Temperature Models, AIAA J., vol. 1, no. 8, Aug. 1963, pp. 1956-1958.

2. Kussoy, M. I.; and Horstman, C. C.: An Experimental Documentation of a Shock-Wave Turbulent Boundary Layer Interaction Flow—With and Without Separation. NASA TMX-62,412, Feb. 1975.

3. Kussoy, M. I.; and Horstman, C. C.: Documentation of Two- and Three-Dimensional Hypersonic Shock Wave/Turbulent Boundary Layer Interaction Flows. NASA TM-101075, Jan. 1989.

4. Behrens, W.: Viscous Interaction Effects on a Static Pressure Probe at M = 6. AIAA J., vol. 1, no. 12, Dec. 1963, pp. 2864-2866.

5. Vas, I. E.: Flow Field Measurements Using a Total Temperature Probe at Hypersonic Speeds. AIAA J., vol. 10, no. 3, Mar. 1972, pp. 317-323.

6. Dudzinski, Thomas J.; and Krause, Lloyd N.: Flow-Direction Measurement With Fixed-Position Probes. NASA TMX-1904, Oct. 1969.

7. Van Driest, E. R.: The Problems of Aerodynamic Heating. Aerospace Engineering Review, 1956, pp. 26-41.

8. Coles, D. E.: The Turbulent Boundary Layer in a Compressible Fluid. Rand Corporation, Report R-403-PR, 1962.

Table 1. Free-stream conditions (x = 187 cm)

$M_\infty = 8.18$

$T_\infty = 81\,K$

$p_\infty = 430\ N/m^2$

$\rho_\infty = 0.0187\ kg/m^3$

$T_w = 300\ K$

$U_\infty = 1446\ m/sec$

$\delta_0 = 3.7\ cm$

$\delta_0^* = 1.59\ cm$

$\theta_0 = 0.094\ cm$

$\tau_{w_\infty} = 19.6\ N/m^2$

$q_{w_\infty} = 10400\ W/m^2$ (wedge flow)*
$= 9900\ W/m^2$ (fin flow)

$Re_{\delta_0} = 1.8 \times 10^5$

$Re_{\theta_0} = 4.6 \times 10^3$

$Re/m = 4.9 \times 10^6$

$$C_{f_\infty} = \frac{\tau_{w_\infty}}{1/2\rho_\infty U_\infty^2} = 0.98 \times 10^{-3}$$

$$C_{h_\infty} = \frac{q_{w_\infty}}{\rho_\infty U_\infty (0.9T_T - T_w)} = 0.53 \times 10^{-3} \text{ (fin flow)}$$

*x = 162 cm.

Table 2. Upstream boundary layer

Y (cm)	M	P/P INF	RHO/ RHO INF	T/T INF	U/U INF	RHOU/ RHOU INF	TT/TT INF
0.000	0.000	1.000	0.270	3.699	0.000	0.000	0.270
0.070	1.777	1.000	0.213	4.705	0.481	0.102	0.555
0.140	2.069	1.000	0.195	5.138	0.584	0.114	0.682
0.200	2.647	1.000	0.237	4.217	0.678	0.161	0.721
0.280	3.083	1.000	0.266	3.756	0.746	0.199	0.773
0.360	3.409	1.000	0.295	3.390	0.784	0.231	0.798
0.430	3.558	1.000	0.301	3.323	0.810	0.244	0.828
0.500	3.747	1.000	0.333	3.002	0.811	0.270	0.808
0.710	4.068	1.000	0.345	2.897	0.864	0.298	0.877
0.920	4.422	1.000	0.386	2.593	0.889	0.343	0.894
1.120	4.750	1.000	0.419	2.388	0.916	0.384	0.922
1.320	5.106	1.000	0.453	2.205	0.947	0.429	0.956
1.520	5.461	1.000	0.504	1.982	0.960	0.484	0.963
1.720	5.774	1.000	0.560	1.785	0.963	0.539	0.956
1.920	6.101	1.000	0.600	1.668	0.984	0.590	0.981
2.130	6.411	1.000	0.671	1.490	0.977	0.656	0.959
2.320	6.689	1.000	0.705	1.419	0.995	0.701	0.983
2.510	7.009	1.000	0.768	1.302	0.998	0.767	0.981
2.710	7.246	1.000	0.820	1.220	0.999	0.819	0.977
3.040	7.617	1.000	0.865	1.156	1.023	0.884	1.012
3.380	7.978	1.000	0.944	1.060	1.025	0.968	1.011
3.730	8.180	1.000	1.000	1.000	1.021	1.021	1.000
4.070	8.180	1.000	0.995	1.005	1.024	1.019	1.004

Table 3. Wedge geometry and orientation

θ (deg)	θ_m (deg)	θ* (deg)	X_o (cm)
5	5	0	104-124
8	10	2	119-135
9	10	1	119-135
10	10	0	124-140
11	15	4	130-145

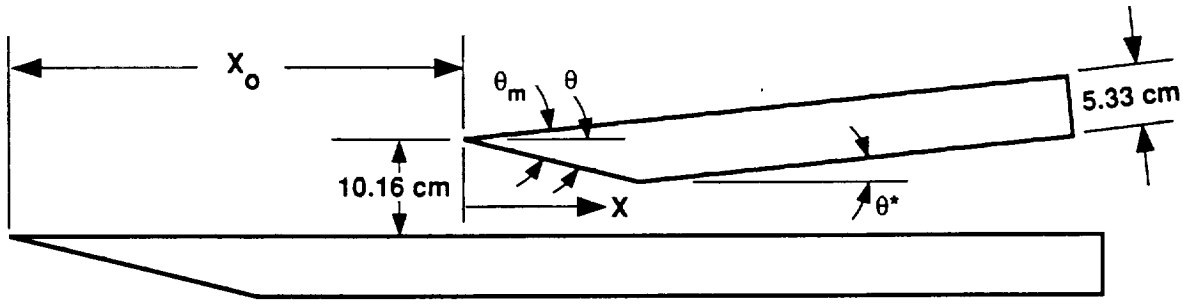

Table 4. Surface pressures

(a) 5° Wedge angle

X (cm)	P/P INF	X (cm)	P/P INF	X (cm)	P/P INF
31.36	0.998	46.60	3.210	56.76	6.016
32.36	1.038	47.60	3.645	57.76	6.161
33.36	1.064	48.60	3.968	58.76	6.306
34.35	1.006	49.59	4.242	59.75	6.387
35.35	1.074	50.59	4.419	60.75	6.516
36.38	1.089	51.62	4.823	61.78	6.613
37.36	1.094	52.60	4.952	62.76	6.677
38.36	1.043	53.60	5.194	63.76	6.774
39.36	1.032	54.60	5.323	64.76	6.871
40.36	1.036	55.60	5.548	65.76	6.952
41.36	1.043	56.60	5.629	66.76	7.048
42.36	1.264	57.60	5.903	67.76	7.065
43.35	1.845	58.59	6.016	68.75	7.113
44.35	2.321	59.59		69.75	7.113
45.35	3.434	60.59	6.258	70.75	7.161
46.35		61.59		71.75	7.177
47.35	4.226	62.59	6.516	72.75	7.161

(b) 8° Wedge angle

X (cm)	P/P INF	X (cm)	P/P INF
26.28	1.013	41.52	13.073
27.28	0.997	42.52	13.600
28.28	1.013	43.52	14.239
29.27	1.016	44.51	14.383
30.27	1.110	45.51	14.367
31.30	1.517	46.54	13.424
32.28	1.825	47.52	12.082
33.28	2.746	48.52	10.803
34.28	4.175	49.52	9.621
35.28		50.52	
36.28	7.556	51.52	7.751
37.28	8.889	52.52	6.952
38.27	10.111	53.51	6.313
39.27	11.222	54.51	5.705
40.27	12.302	55.51	5.242
41.27	13.190	56.51	4.826
42.27	13.619	57.51	4.427

Table 4. Continued

(c) 9° Wedge angle

X (cm)	P/P INF	X (cm)	P/P INF
26.28	1.008	41.52	18.681
27.28	1.048	42.52	19.173
28.28	1.210	43.52	19.173
29.27	1.484	44.51	17.862
30.27	1.855	45.51	15.994
31.30	2.339	46.54	13.995
32.28	3.194	47.52	12.290
33.28	5.081	48.52	10.865
34.28	7.290	49.52	9.652
35.28		50.52	
36.28	11.258	51.52	7.800
37.28	12.968	52.52	7.014
38.27	14.532	53.51	6.391
39.27	15.710	54.51	5.817
40.27	16.774	55.51	5.391
41.27	17.419	56.51	4.998
42.27	18.065	57.51	4.605

(d) 10° Wedge angle

X (cm)	P/P INF	X (cm)	P/P INF	X (cm)	P/P INF
21.20	1.040	21.20	1.048	41.52	21.396
22.20	0.985	22.20	1.016	42.52	21.396
23.20	1.018	23.20	1.008	43.52	19.480
24.19	1.037	24.19	1.018	44.51	17.085
25.19	1.000	25.19	1.108	45.51	14.946
26.22	1.152	26.22	1.468	46.54	12.998
27.20	1.392	27.20	1.855	47.52	11.305
28.20	1.790	28.20	2.274	48.52	9.932
29.20	2.081	29.20	2.710	49.52	8.814
30.20	2.726	30.20		50.52	7.888
31.20	3.597	31.20	4.774	51.52	7.074
32.20	5.452	32.20	6.677	52.52	6.435
33.19	7.726	33.19	8.903	53.51	5.860
34.19	9.048	34.19	11.113	54.51	4.615
35.19	12.290	35.19	13.274	55.51	4.950
36.19	14.629	36.19	15.419	56.51	4.678
37.19	16.613	37.19	17.258	57.51	4.295

Table 4. Concluded

(e) 11° Wedge angle

X (cm)	P/P INF	X (cm)	P/P INF
16.12	1.040	31.36	21.420
17.12	1.068	32.36	20.325
18.12	1.302	33.36	18.136
19.11	1.635	34.35	16.104
20.11	1.968	35.35	14.024
21.14	2.381	36.38	12.336
22.12	2.984	37.36	10.819
23.12	3.825	38.36	9.600
24.12	4.952	39.36	8.599
25.12		40.36	
26.12	8.746	41.36	6.957
27.12	11.016	42.36	6.379
28.11	13.270	43.35	5.863
29.11	15.524	44.35	5.410
30.11	17.937	45.35	5.019
31.11	19.683	46.35	4.784
32.11	19.365	47.35	4.346

Table 5. Heat transfer

(a) 5° Wedge angle

Thermocouples

X (cm)	Q/Q INF	X (cm)	Q/Q INF	X (cm)	Q/Q INF
36.44	0.94	46.60	2.81	56.76	4.02
37.42	0.92	47.58	3.21	57.74	4.16
38.43	0.93	48.59	3.54	58.75	4.27
39.41	0.95	49.57	3.71	59.73	4.37
40.37	0.94	50.53	3.85	60.69	4.45
41.36	0.94	51.52	3.86	61.68	4.51
42.36	0.95	52.52	4.03	62.68	4.52
43.37	0.97	53.53	4.03	63.69	4.58
45.39	1.50	55.55	4.26	65.71	4.67
46.39	2.10	56.55	4.28	66.71	4.69
47.39	2.71	57.55	4.30	67.71	4.50
49.65	3.61	59.81	4.55	69.97	4.62
50.40	3.75	60.56	4.46	70.72	4.61
52.44	4.00	62.60	4.61	72.76	4.47

Schmidt-Boelter gauges

X (cm)	Q/Q INF	X (cm)	Q/Q INF	X (cm)	Q/Q INF
36.34	1.07	46.50	2.80	56.66	4.79
38.14	0.96	48.30		58.46	4.64
39.94		50.10	3.96	60.26	
41.74	0.97	51.90	3.95	62.06	4.73
43.54	1.01	53.70		63.86	5.33
45.34	1.53	55.50	4.28	65.66	5.16
47.14	2.68	57.30	4.61	67.46	5.30
48.94	3.52	59.10	4.84	69.26	4.72
50.74	3.41	60.90	4.73	71.06	4.79
52.54	3.76	62.70	5.06	72.86	5.78

Table 5. Continued

(b) 8° Wedge angle

Thermocouples				Schmidt-Boelter gauges			
X (cm)	Q/Q INF	X (cm)	Q/Q INF	X (cm)	Q/Q INF	X (cm)	Q/Q INF
26.28	0.99	41.52	8.99	26.18	1.27	41.42	8.73
27.26	1.01	42.50	9.49	27.98	1.14	43.22	8.87
28.27	1.01	43.51	9.82	29.78	3.41	45.02	
29.25	1.01	44.49	9.64	31.58		46.82	7.78
30.21	0.98	45.45	9.72	33.38		48.62	7.75
31.20	0.88	46.44	9.48	35.18	5.71	50.42	5.93
32.20	0.91	47.44	8.66	36.98	7.73	52.22	5.16
33.21	1.38	48.45	7.71	38.78	8.74	54.02	3.00
35.23	5.08	50.47	6.26	40.58	8.83	55.82	3.75
36.23	6.62	51.47	5.73	42.38	9.65	57.62	5.16
37.23	7.04	52.47	4.93				
39.49	8.31	54.73	4.17				
40.24	8.33	55.48	3.74				
42.28	9.20	57.52	3.25				

(c) 9° Wedge angle

Thermocouples				Schmidt-Boelter gauges			
X (cm)	Q/Q INF	X (cm)	Q/Q INF	X (cm)	Q/Q INF	X (cm)	Q/Q INF
26.28	1.18	41.52	11.53	26.18	1.07	41.42	10.73
27.26	1.24	42.50	12.12	27.98	0.96	43.22	10.83
28.27	1.14	43.51	12.12	29.78		45.02	
29.25	0.99	44.49	11.13	31.58	1.30	46.82	7.61
30.21	0.97	45.45	10.14	33.38	4.55	48.62	7.58
31.20	1.33	46.44	9.39	35.18	7.02	50.42	5.75
32.20	2.38	47.44	8.32	36.98	7.85	52.22	4.96
33.21	4.44	48.45	7.44	38.78	8.66	54.02	2.93
35.23	8.33	50.47	5.93	40.58	9.19	55.82	3.69
36.23	9.21	51.47	5.44	42.38	10.13	57.62	4.99
37.23	9.01	52.47	4.69				
39.49	11.04	54.73	4.04				
40.24	10.84	55.48	3.58				
42.28	11.75	57.52	3.17				

Table 5. Continued

(d) 10° Wedge angle

Thermocouples

X (cm)	Q/Q INF	X (cm)	Q/Q INF	X (cm)	Q/Q INF
21.20	1.01	21.20	0.94	41.52	13.61
22.18	1.03	22.18	0.93	42.50	13.61
23.19	1.05	23.19	0.95	43.51	12.71
24.17	1.00	24.17	0.96	44.49	11.31
25.13	1.01	25.13	0.95	45.45	9.98
26.12	1.01	26.12		46.44	9.71
27.12	0.89	27.12	0.88	47.44	7.79
28.13	0.87	28.13	0.72	48.45	6.29
30.15	1.76	30.15	1.42	50.47	5.53
31.15	3.14	31.15	2.39	51.47	4.76
32.15	5.21	32.15	4.39	52.47	4.46
34.41	9.04	34.41	8.73	54.73	3.82
35.16	9.37	35.16	9.15	55.48	3.47
37.20	10.86	37.20	10.60	57.52	2.98

Schmidt-Boelter gauges

X (cm)	Q/Q INF	X (cm)	Q/Q INF	X (cm)	Q/Q INF
21.10	1.34	21.10	0.92	41.42	10.81
22.90	1.21	22.90		43.22	15.21
24.70		24.70	0.94	45.02	8.88
26.50	1.19	26.50	0.95	46.82	6.91
28.30	1.12	28.30		48.62	
30.10	1.98	30.10	1.26	50.42	4.81
31.90	5.18	31.90	3.45	52.22	4.37
33.70	10.56	33.70	6.90	54.02	3.82
35.50	10.36	35.50	8.18	55.82	3.25
37.30	10.36	37.30	9.79	57.62	3.07

Table 5. Concluded

(e) 11° Wedge angle

Thermocouples				Schmidt-Boelter gauges			
X (cm)	Q/Q INF	X (cm)	Q/Q INF	X (cm)	Q/Q INF	X (cm)	Q/Q INF
16.12	1.06	31.36	13.77	16.02	1.06	31.26	12.27
17.10	1.03	32.34	13.13	17.82	0.92	33.06	10.61
18.11	1.02	33.35	11.85	19.62		34.86	6.49
19.09	0.90	34.33	10.22	21.42	1.29	36.66	6.95
20.05	0.96	35.29	9.08	23.22	2.80	38.46	
21.04	1.34	36.28	8.37	25.02	5.44	40.26	5.33
22.04	1.88	37.28	7.39	26.82	8.26	42.06	4.56
23.05	2.68	38.29	6.62	28.62	9.69	43.86	2.60
25.07	5.96	40.31	5.31	30.42	10.74	45.66	3.44
26.07	7.95	41.31	4.90	32.22	11.45	47.46	4.62
27.07	9.08	42.31	4.30				
29.33	11.66	44.57	3.64				
30.08	11.96	45.32	3.27				
32.12	12.17	47.36	2.89				

Table 6. Surface streamline angles on flat plate with fin

10° Fin angle		15° Fin angle	
Z (cm)	α (deg)	Z (cm)	α (deg)
0.20	10.0	0.22	15.0
0.40	15.5	0.68	35.7
0.84	21.3	1.20	44.7
1.28	29.4	1.75	47.2
1.83	34.3	2.12	50.3
2.22	34.8	2.44	50.5
2.63	35.2	2.85	45.2
2.96	30.0	3.30	39.0
3.28	25.0	3.90	27.2
4.30	24.0	4.70	32.8
5.50	23.8	5.40	33.0
6.78	23.2	6.34	32.0
7.59	17.2	7.10	34.2
8.30	10.8	8.75	32.2
8.91	0.0	9.42	27.5
		10.15	7.5
		10.55	0.0

Table 7. Surface pressures on fin (P/P INF)

S = 18.34 cm					
	Fin angle				
Y (cm)	5°	7.5°	10°	12.5°	15°
0.45	1.855	2.565	3.532	4.516	5.871
0.95	1.823	2.484	3.323	4.210	5.274
1.45	1.790	2.452	3.242	4.065	5.000
2.45	1.984	2.839	3.887	5.016	6.484
3.43	2.145	3.290	4.823	6.242	8.306
4.43	2.355	3.613	5.371	7.000	9.355
5.42	2.419	3.774	5.565	7.274	9.677
6.42	2.435	3.855	5.677	7.435	9.839
7.42	2.516	3.903	5.742	7.532	9.968
8.41	2.597	4.032	5.839	7.694	10.161
9.40	2.565	4.016	5.935	7.774	10.306
10.40	2.613	4.145	6.065	7.887	10.468

Table 8. Surface pressures on flat plate with fin

X = 18.19 cm

Fin angle									
5°		7.5°		10°		12.5°		15°	
Z (cm)	P/P INF	Z (cm)	P/P INF	Z (cm)	P/P INF	Z (cm)	P/P INF	Z (cm)	P/P INF
15.82	1.000	15.29	1.089	14.78	1.127	14.27	1.229	13.72	1.021
14.82	0.979	14.29	1.050	13.78	1.102	14.27	1.229	13.72	1.021
13.82	0.968	13.29	1.061	12.78	1.113	13.27	1.213	12.72	1.016
12.83	0.990	12.30	1.050	11.79	1.098	12.27	1.226	11.72	1.037
11.83	0.940	11.30	1.044	10.79	1.121	11.28	1.223	10.73	1.094
10.80	1.027	10.27	1.103	9.76	1.113	10.28	1.252	9.73	1.292
9.82	0.994	9.29	1.065	8.78	1.195	9.25	1.327	8.70	1.529
8.82	0.990	8.29	1.123	7.78	1.363	8.27	1.500	7.72	1.839
7.82	1.008	7.29	1.197	6.78	1.561	7.27	1.726	6.72	2.145
6.82	1.115	6.29	1.358	5.78	1.758	6.27	1.968	5.72	2.339
5.82	1.169	5.29	1.506	4.78	1.968	5.27	2.194	4.72	2.452
4.82	1.324	4.29	1.661	3.78	2.065	4.27	2.371	3.72	2.452
3.83	1.410	3.30	1.774	2.79	2.161	3.27	2.387	2.72	2.613
2.83	1.497	2.30	1.935	1.79	2.742	2.28	2.758	1.73	4.113
1.83	1.608	1.30	2.371	0.79	3.742	1.28	3.984	0.73	6.387
0.83	2.000	0.30	2.887			0.28	5.065		

Table 9. Heat transfer on fin (Q/Q INF)

Thermocouples, S = 16.70 cm

	Fin Angle				
Y (cm)	5°	7.5°	10°	12.5°	15°
0.47	1.28	2.06	3.04	3.82	5.01
0.95	1.17	1.80	2.86	3.47	4.24
1.45	1.30	2.11	2.99	3.69	4.55
2.45	1.40	2.37	3.27	4.20	5.50
3.45	1.44	2.32	3.02	3.83	5.30
4.45	1.43	1.98	2.54	2.90	4.02
5.45	1.30	1.85	2.31	2.60	3.35
6.43	1.25	1.68	2.07	2.35	3.05
7.43	1.19	1.65	2.03	2.41	3.09
8.43	1.20	1.69	2.06	2.38	3.08
9.40	1.21	1.67	2.04	2.39	2.93
10.38	1.16	1.67	2.02	2.42	2.94

Schmidt-Boelter gauges, S = 19.62 cm

	Fin Angle				
Y (cm)	5°	7.5°	10°	12.5°	15°
2.45	1.34	1.65	2.61	3.43	4.28
3.45	1.39	1.66	2.61	3.54	4.74
4.43	1.43	1.64	2.40	3.12	4.26
5.42	1.30	1.51	2.18	2.77	3.69
7.15	1.06	1.23	1.74	2.31	3.01
9.15	1.17	1.38	1.91	2.57	3.26

Table 10. Heat transfer on flat plate with fin

X = 16.45 cm

Fin Angle									
5°		7.5°		10°		12.5°		15°	
Z (cm)	Q/Q INF	Z (cm)	Q/Q INF	Z (cm)	Q/Q INF	Z (cm)	Q/Q INF	Z (cm)	Q/Q INF
15.75	0.86	15.27	0.95	14.76	0.99	14.35	0.99	13.89	0.98
14.77	0.96	14.29	0.99	13.78	1.02	13.37	1.01	12.91	1.00
13.76	0.94	13.28	1.06	12.77	1.05	12.36	1.02	11.90	1.03
12.78	0.95	12.30	1.03	11.79	1.05	11.38	1.01	10.92	1.00
11.82	0.92	11.34	1.01	10.83	1.07	10.42	1.02	9.96	0.94
10.83	0.96	10.35	1.06	9.84	1.08	9.43	1.06	8.97	0.95
9.82	0.98	9.34	1.10	8.83	1.07	8.42	1.00	7.96	0.95
8.82	0.98	8.34	1.03	7.83	1.04	7.42	0.95	6.96	1.46
6.80	0.96	6.32	1.03	5.81	1.20	5.40	1.58	4.94	2.01
5.80	1.05	5.32	1.18	4.81	1.58	4.40	1.85	3.94	1.80
4.80	1.11	4.32	1.30	3.81	1.58	3.40	1.56	2.94	1.75
2.54	1.29	2.06	1.87	1.55	2.61	1.14	3.54	0.68	4.96
1.79	1.47	1.31	2.31	0.80	3.23	0.39	4.07		

Table 11. Flow field yaw angles (degrees)

(a) 10° Fin angle

X = 17.23 cm

	Z (cm)					
Y (cm)	0.64	1.27	1.91	2.54	3.81	5.08
0.00	16	25	35	35	25	24
0.25	14	17	20	22	21	15
0.50	14	15	18	19	15	9
0.75	13	14	16	15	10	4
1.00	13	13	14	11	5	2
1.25	13	12	12	7	2	1
1.50	12	11	10	5	1	1
1.75	12	11	9	3	0	0
2.00	12	10	9	2	0	0
2.25	11	10	9	2	0	0
2.50	11	10	9	2	0	0
2.75	11	10	9	2	0	0
3.00	11	10	10	2	0	0
3.25	11	10	11	2	0	0

(b) 15° Fin angle

X = 17.44 cm

	Z (cm)						
Y (cm)	1.27	1.91	2.54	3.81	5.08	6.35	7.62
0.00	44	46	50	37	33	32	34
0.25	25	23	32	33	32	25	14
0.50	22	21	30	29	27	17	7
0.75	21	20	26	23	19	9	3
1.00	19	18	20	17	11	5	2
1.25	18	16	12	10	5	2	1
1.50	17	13	7	4	2	1	1
1.75	16	10	2	1	1	0	0
2.00	15	8	1	0	0	0	0
2.25	14	3	1	0	0	0	0
2.50	14	1	0	0	0	0	0
2.75	14		1	0	0	0	0
3.00	14		1	0	0	0	0
3.25	15		1	0	0	0	0

Table 12. Flow field pitot pressures (PT2/PT2 INF)

(a) 10° Fin angle

X = 17.23 cm

	Z (cm)					
Y (cm)	0.64	1.27	1.91	2.54	3.81	5.08
0.25	0.51	0.51	0.40	0.33	0.16	0.15
0.50	0.70	0.60	0.39	0.31	0.20	0.20
0.75	0.85	0.63	0.38	0.30	0.24	0.28
1.00	0.95	0.69	0.42	0.33	0.32	0.35
1.25	1.04	0.75	0.48	0.39	0.41	0.44
1.50	1.16	0.84	0.57	0.49	0.51	0.55
1.75	1.26	0.96	0.70	0.61	0.64	0.62
2.00	1.44	1.11	0.86	0.76	0.78	0.71
2.25	1.61	1.27	1.07	0.95	0.88	0.75
2.50	1.79	1.48	1.31	1.15	0.89	0.80
2.75	1.97	1.71	1.67	1.33	0.91	0.85
3.00	2.15	1.96	1.97	1.40	0.93	0.89
3.25	2.47	2.21	2.32	1.32	0.94	0.95

(b)15° Fin angle

X = 17.44 cm

	Z (cm)						
Y (cm)	1.27	1.91	2.54	3.81	5.08	6.35	7.62
0.25	0.88	0.62	0.44	0.36	0.20	0.17	0.13
0.50	0.93	0.59	0.41	0.34	0.24	0.20	0.21
0.75	0.90	0.52	0.33	0.31	0.27	0.27	0.29
1.00	0.88	0.47	0.30	0.29	0.33	0.36	0.37
1.25	0.91	0.47	0.33	0.33	0.41	0.47	0.44
1.50	0.99	0.53	0.40	0.42	0.54	0.59	0.50
1.75	1.15	0.63	0.54	0.58	0.70	0.70	0.56
2.00	1.31	0.97	0.70	0.74	0.86	0.74	0.61
2.25	1.58	0.96	0.89	0.96	0.97	0.75	0.68
2.50	1.86	1.17	1.12	1.14	0.95	0.79	0.75
2.75	2.23		1.35	1.15	0.89	0.86	0.83
3.00	2.49		1.38	1.06	0.93	0.90	0.87
3.25	2.79		1.22	0.98	0.98	0.95	0.93

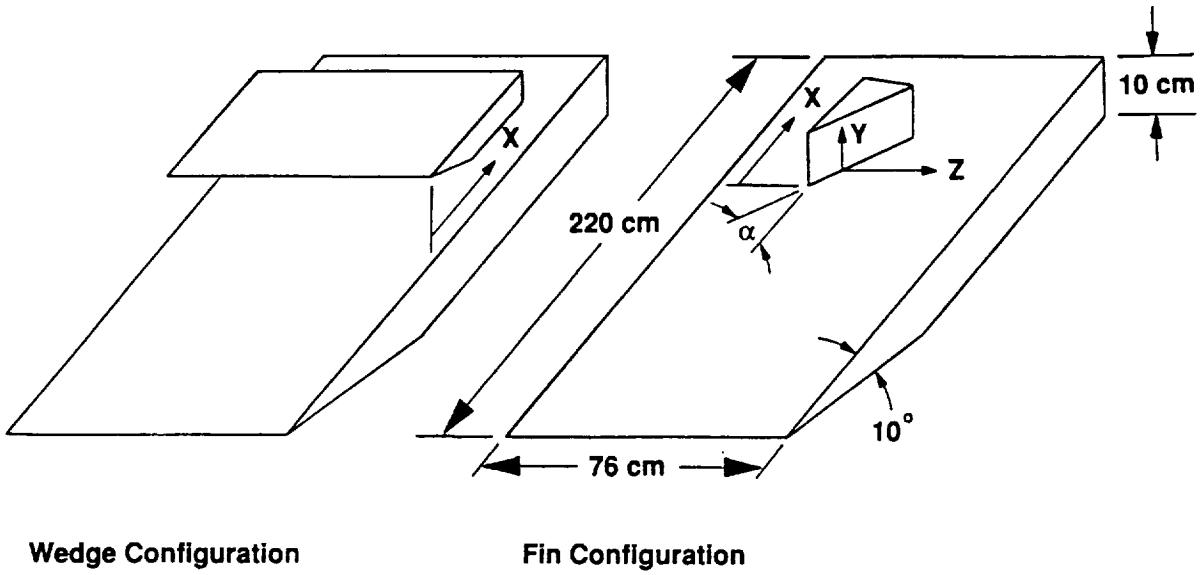

Figure 1. Test body configurations and coordinate systems used.

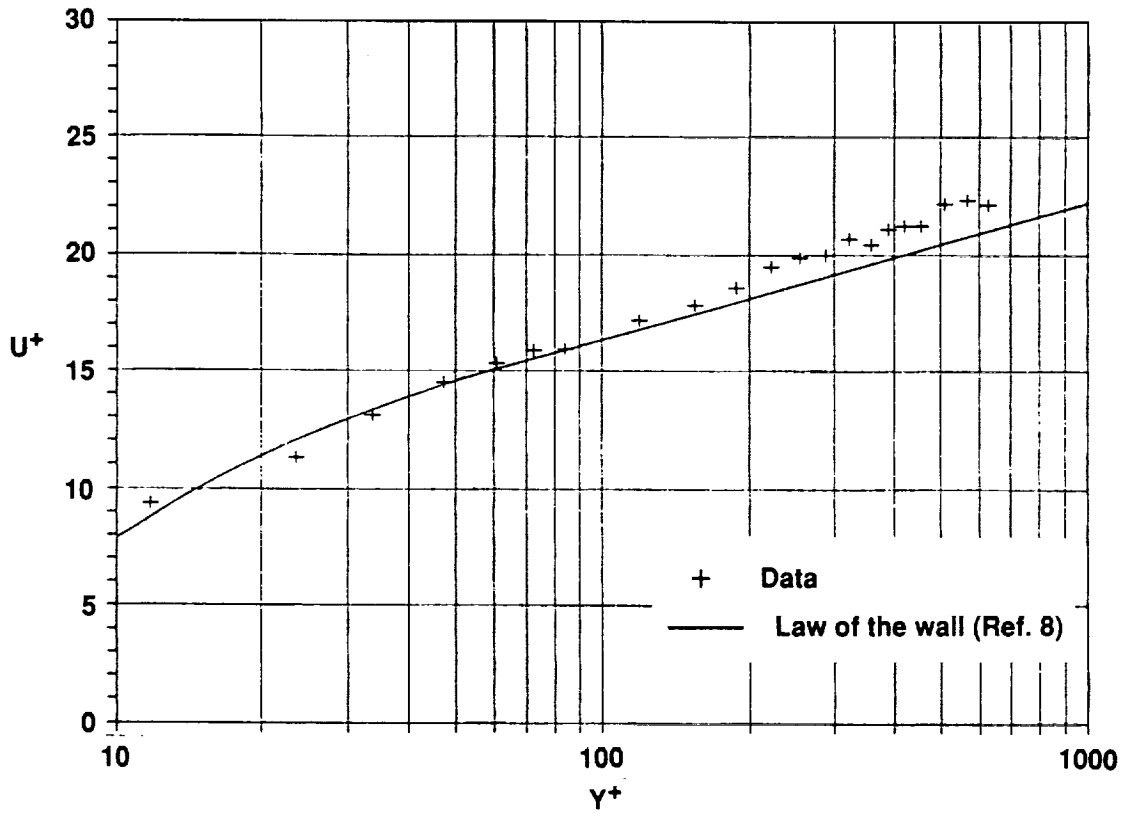

Figure 2. Mean velocity distributions in law-of-the-wall coordinates for the undisturbed boundary layer.

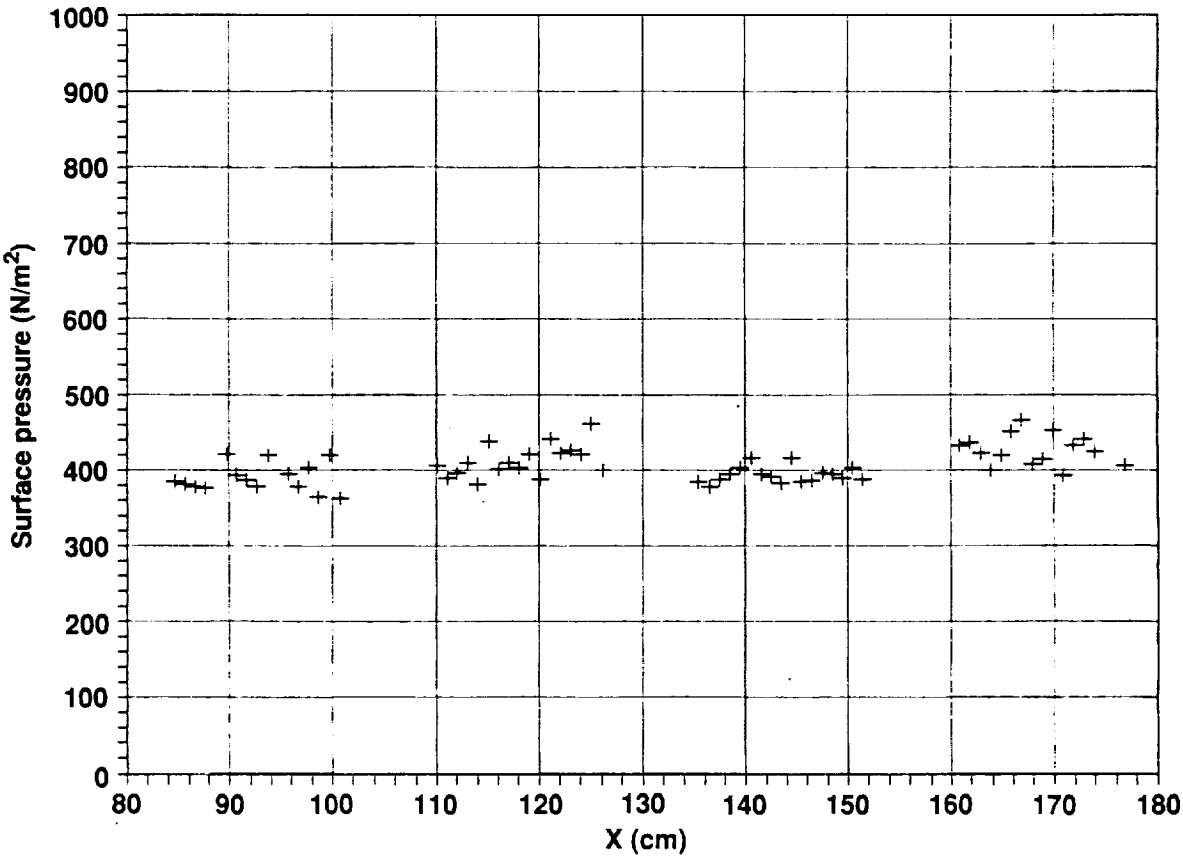

Figure 3. Longitudinal variation of surface pressure on flat plate (undisturbed boundary layer).

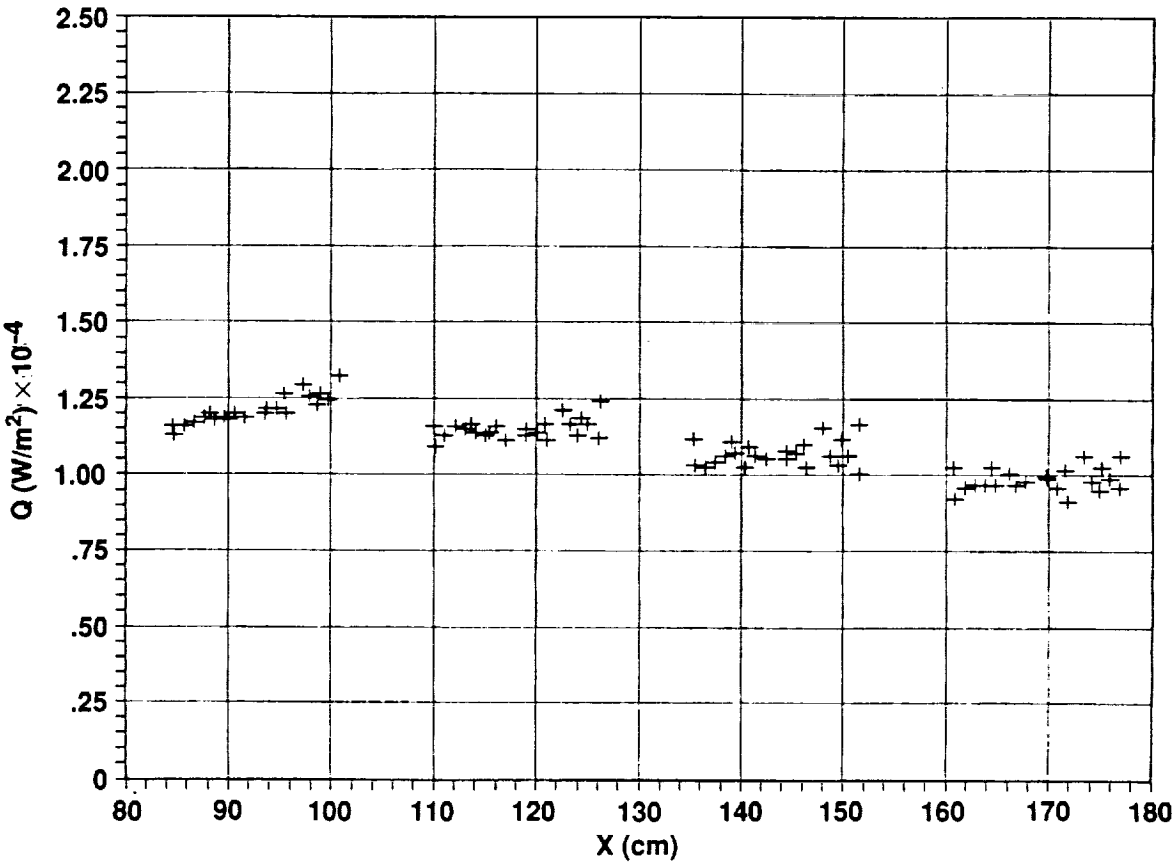

Figure 4. Longitudinal variation of heat transfer on flat plate (undisturbed boundary layer).

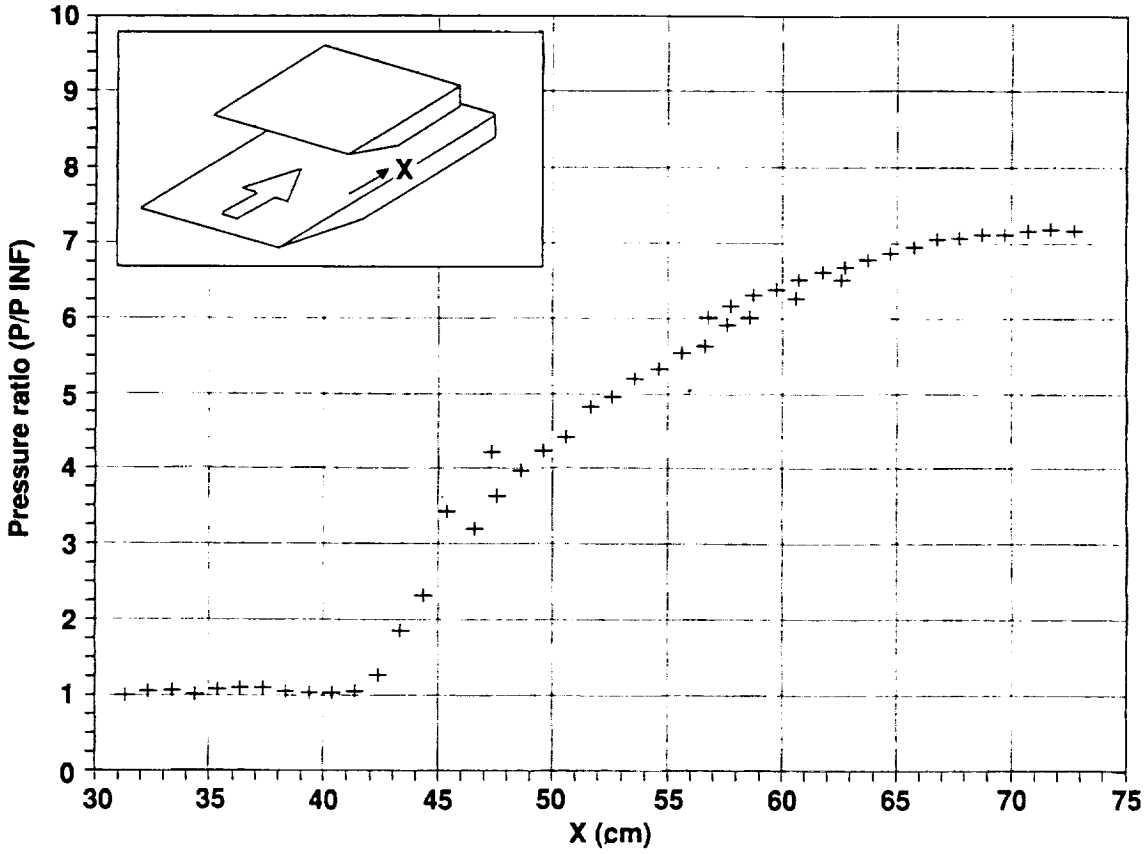

Figure 5. Surface pressure distribution. (a) 5° wedge angle.

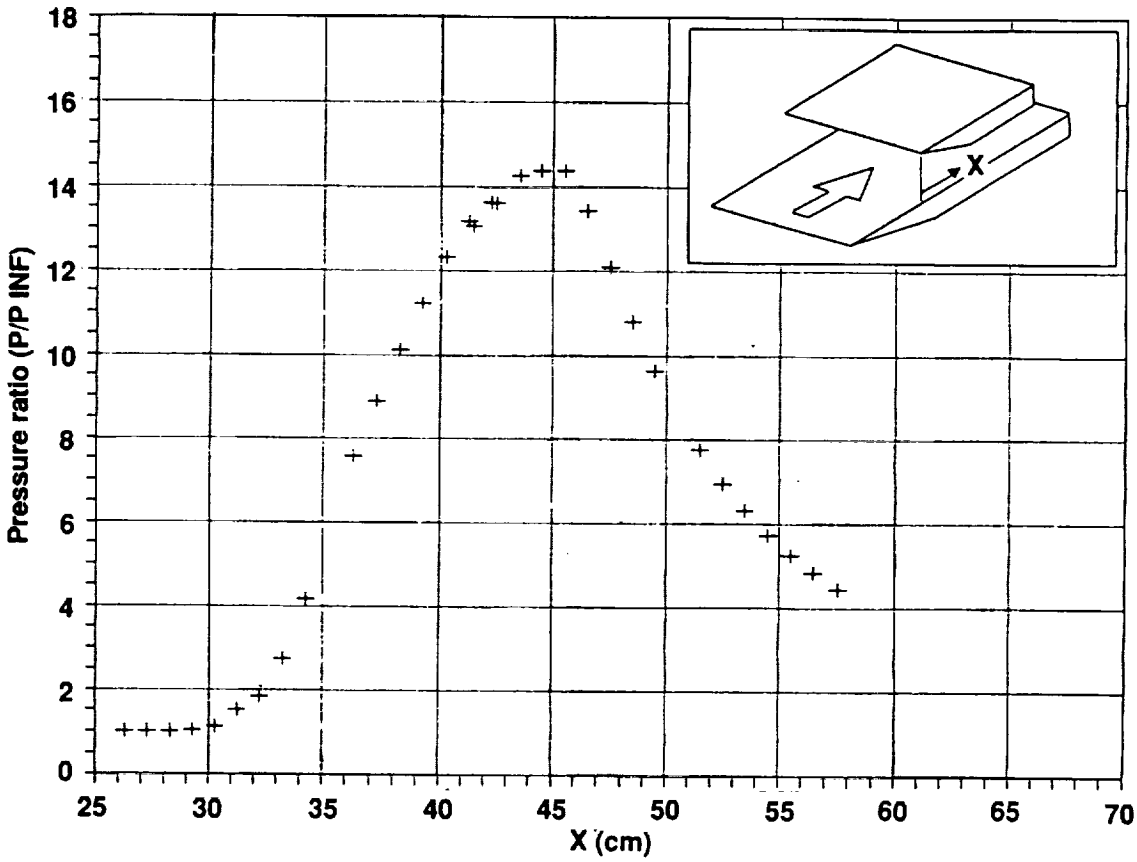

Figure 5. Continued. (b) 8° wedge angle.

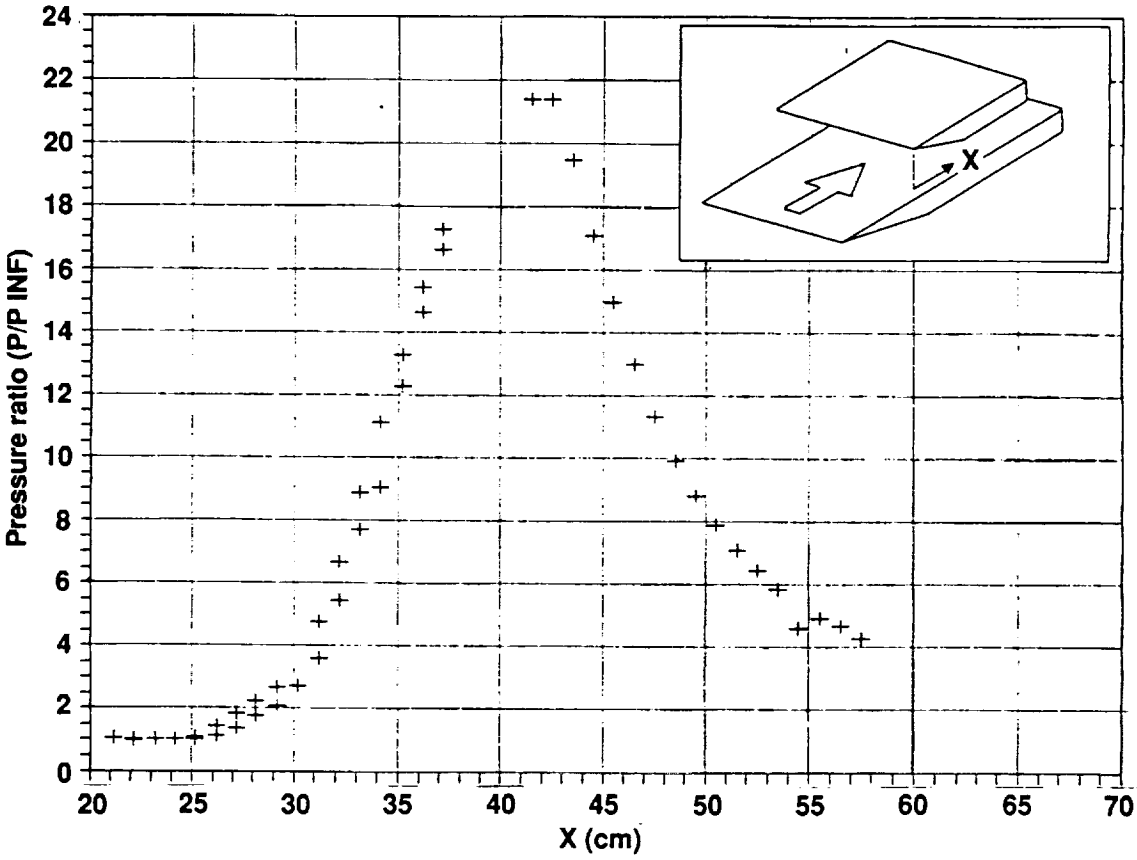

Figure 5. Concluded. (c) 10° wedge angle.

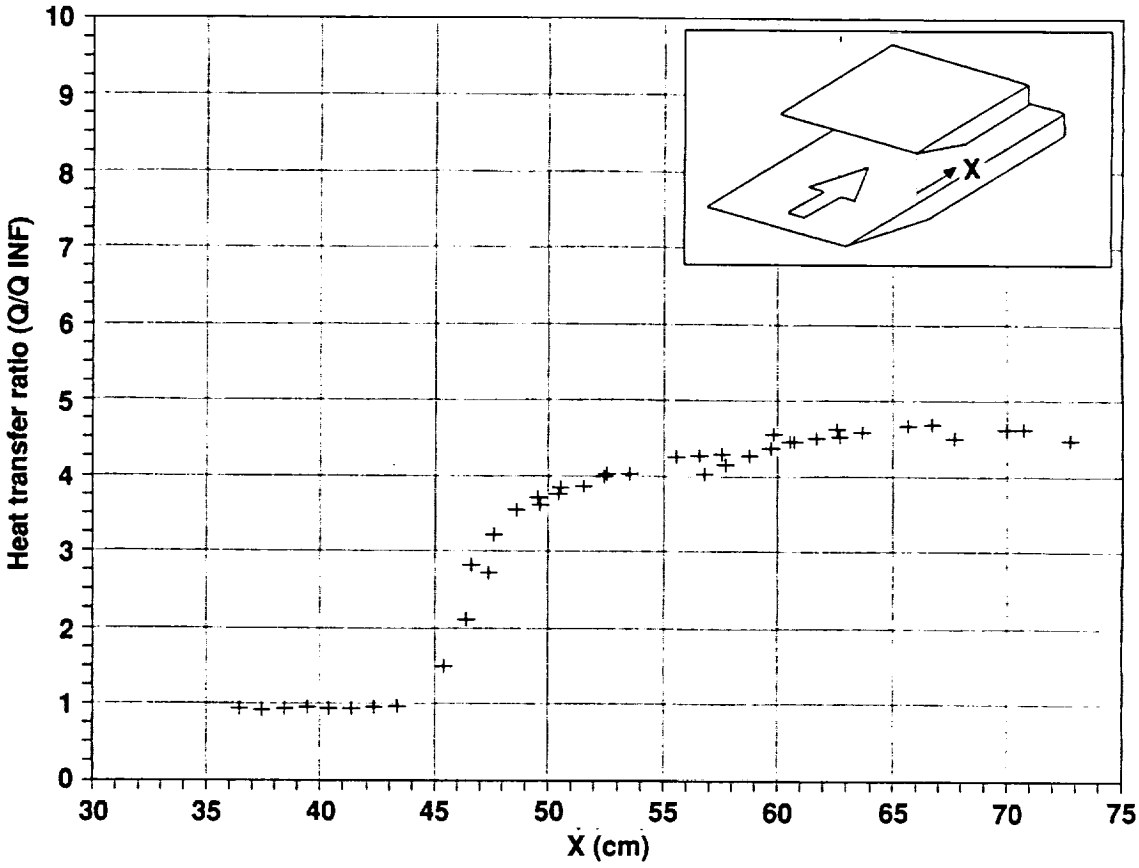

Figure 6. Heat transfer distribution. (a) 5° wedge angle.

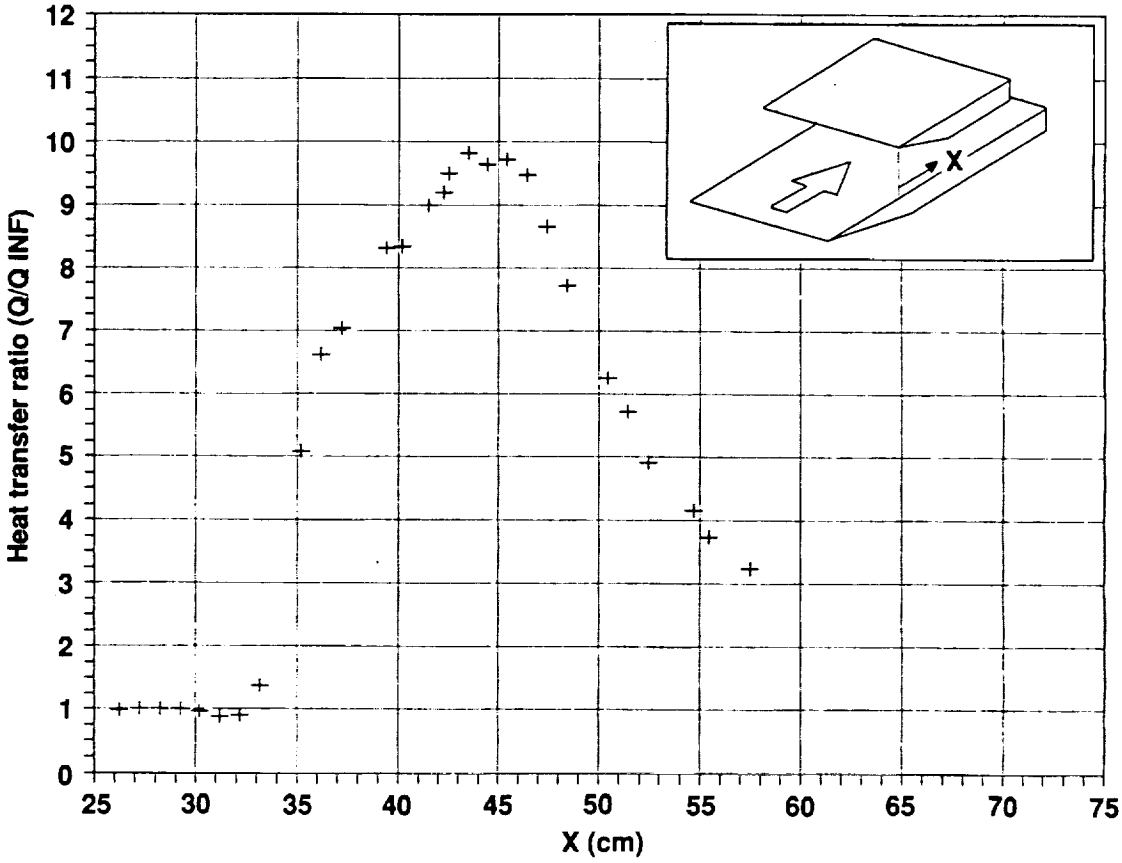

Figure 6. Continued. (b) 8° wedge angle.

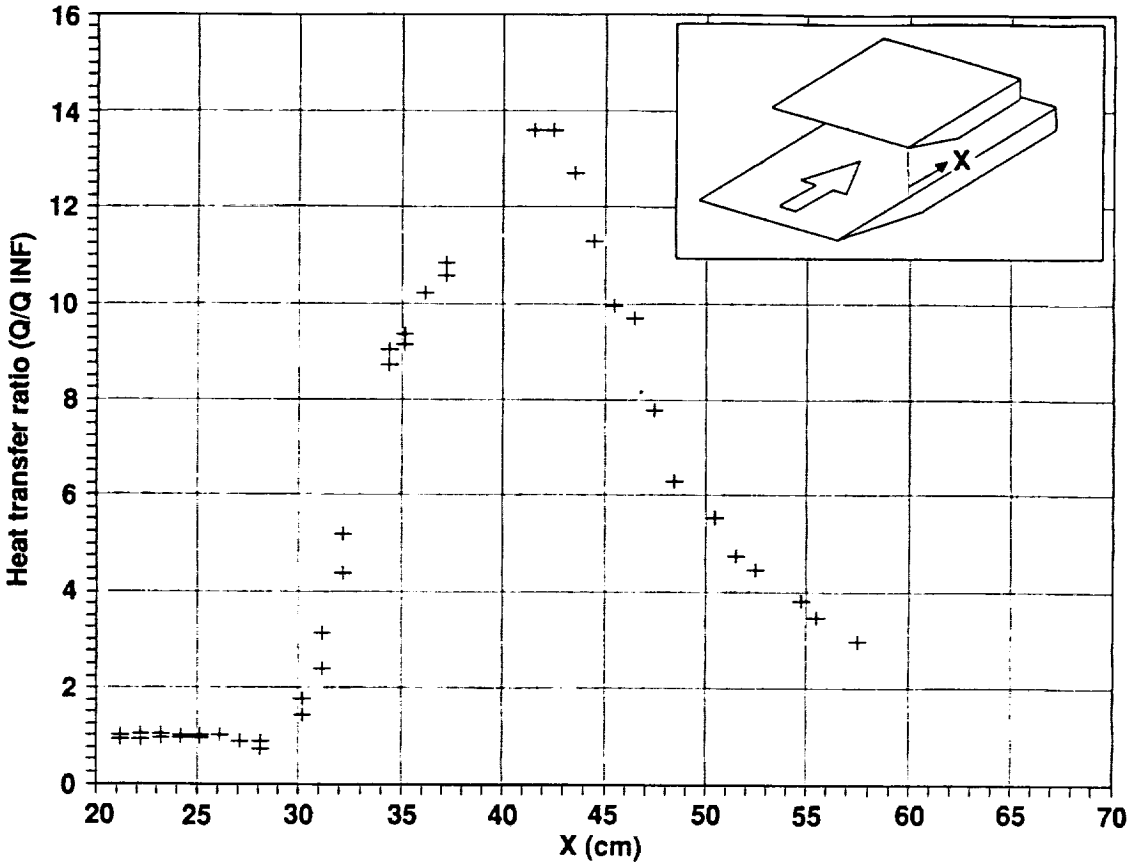

Figure 6. Concluded. (c) 10° wedge angle.

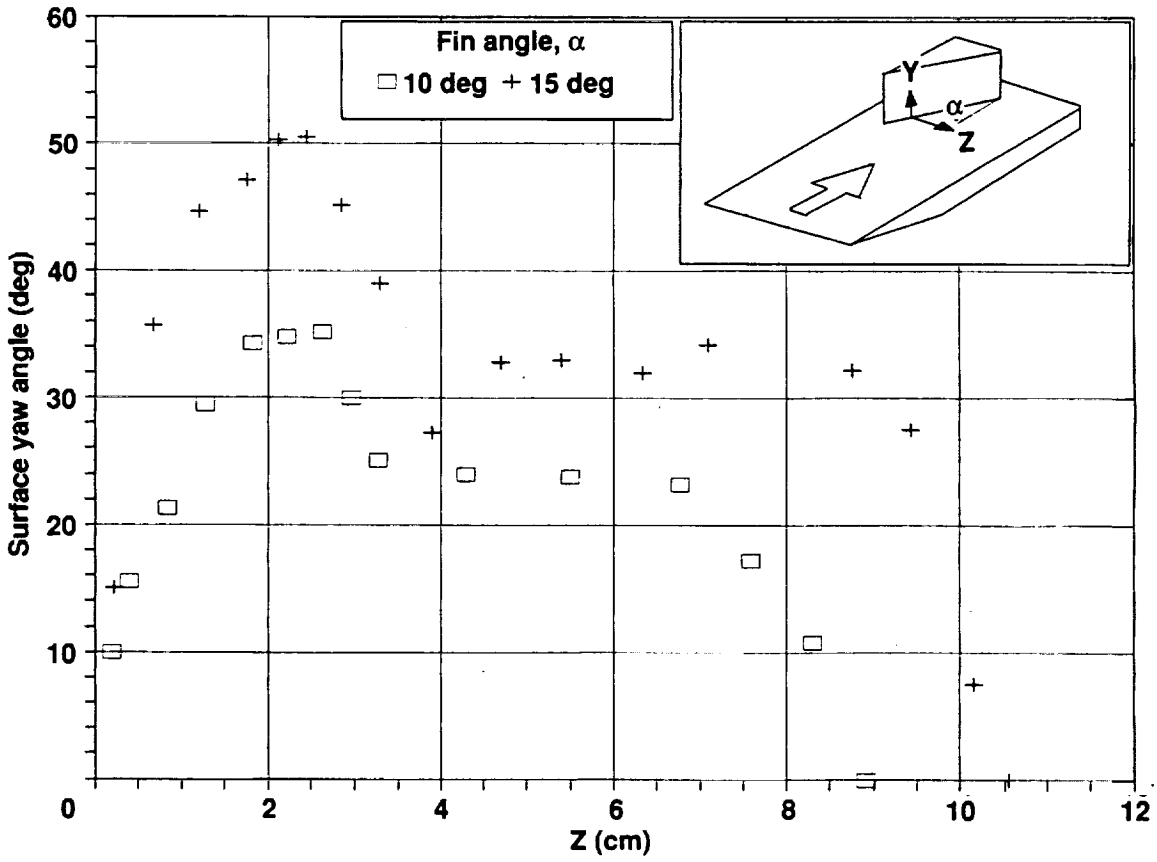

Figure 7. Surface yaw angle distribution at X = 16.5 cm.

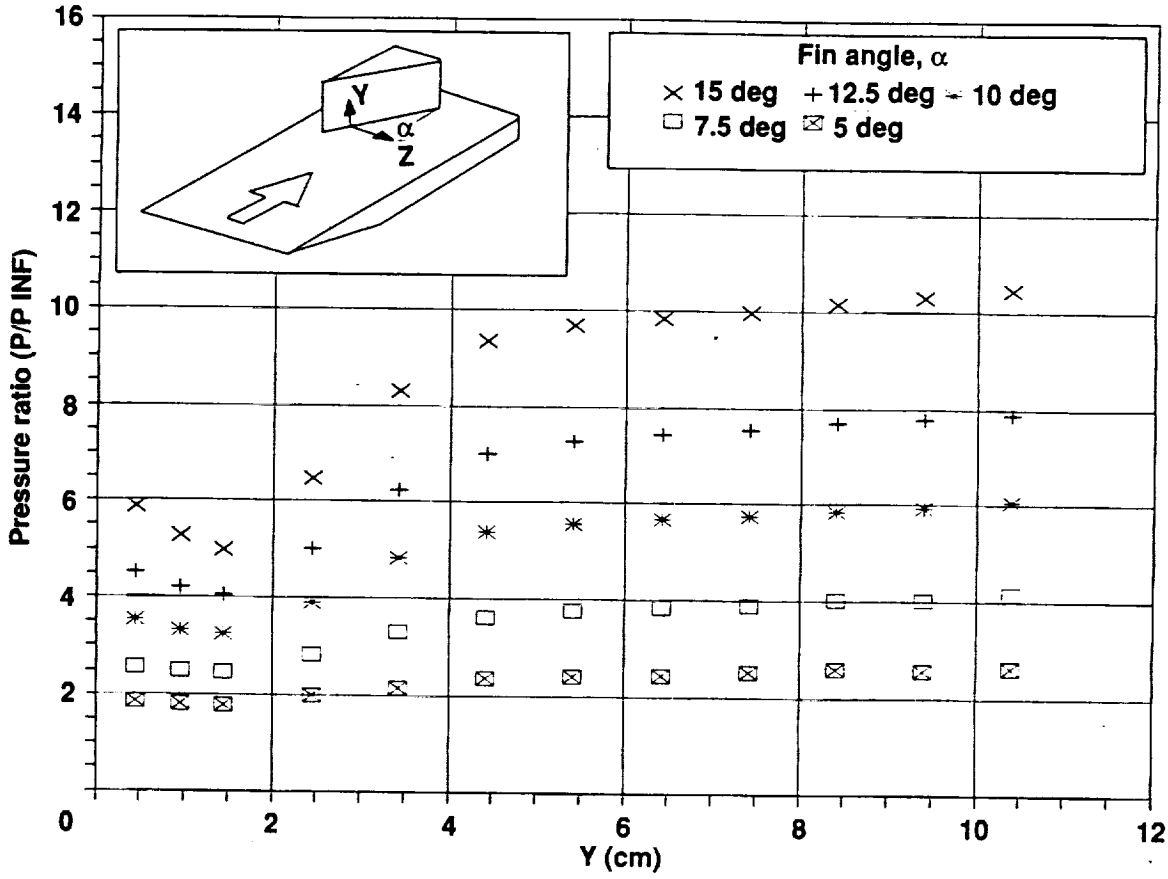

Figure 8. Surface pressure distribution on fin.

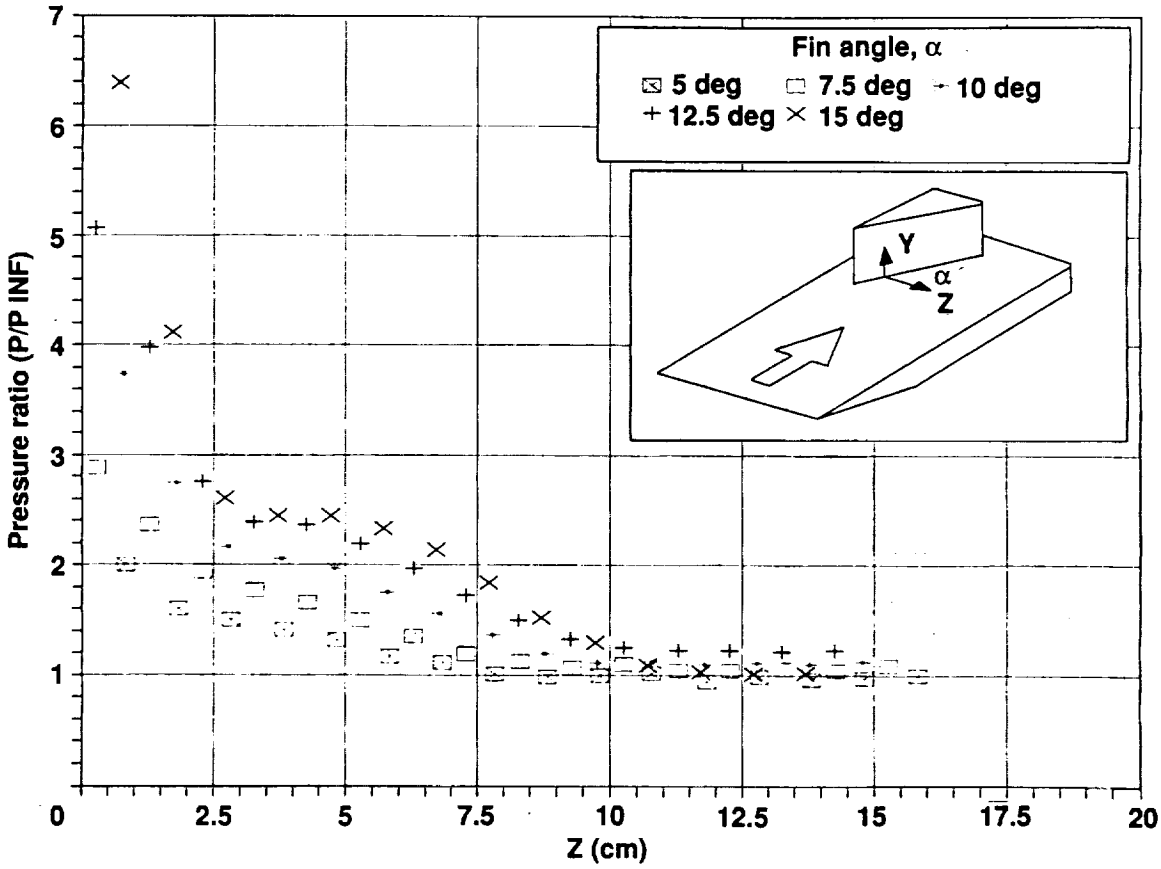

Figure 9. Surface pressure distribution on flat plate.

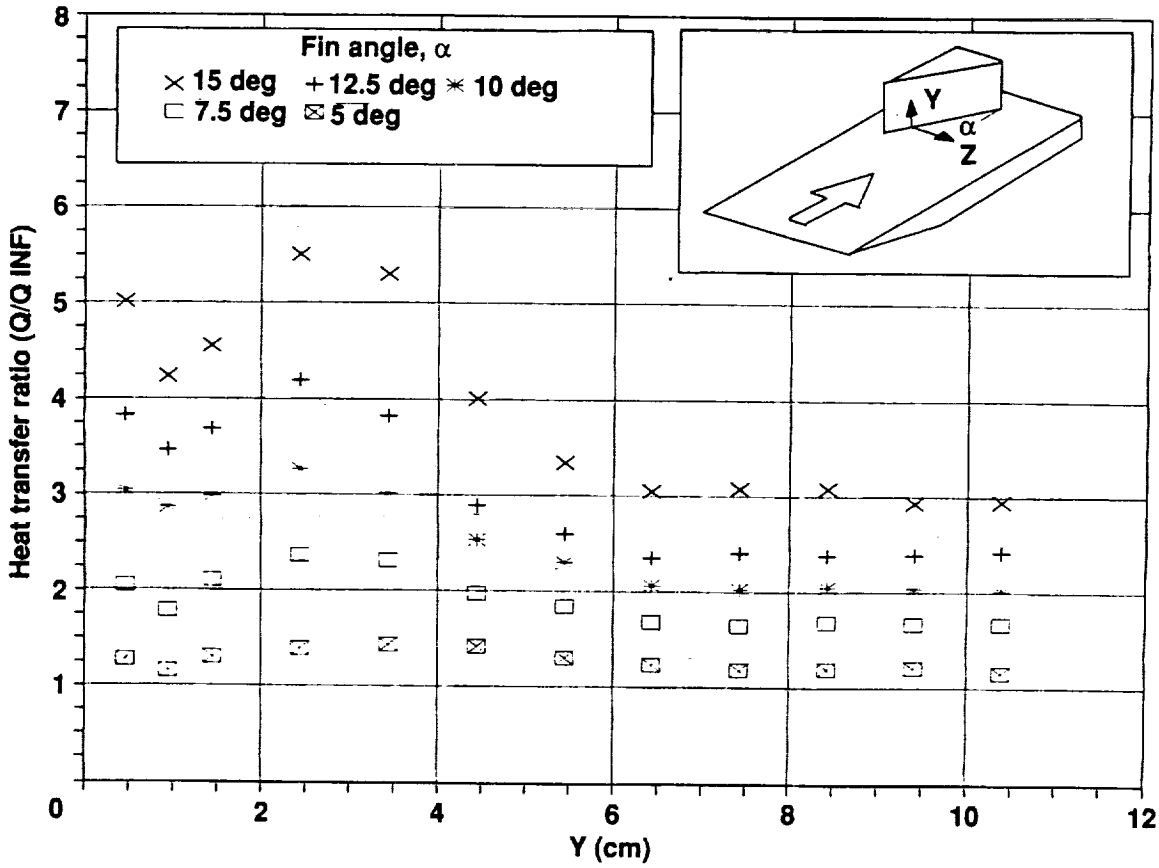

Figure 10. Heat transfer distribution on fin surface.

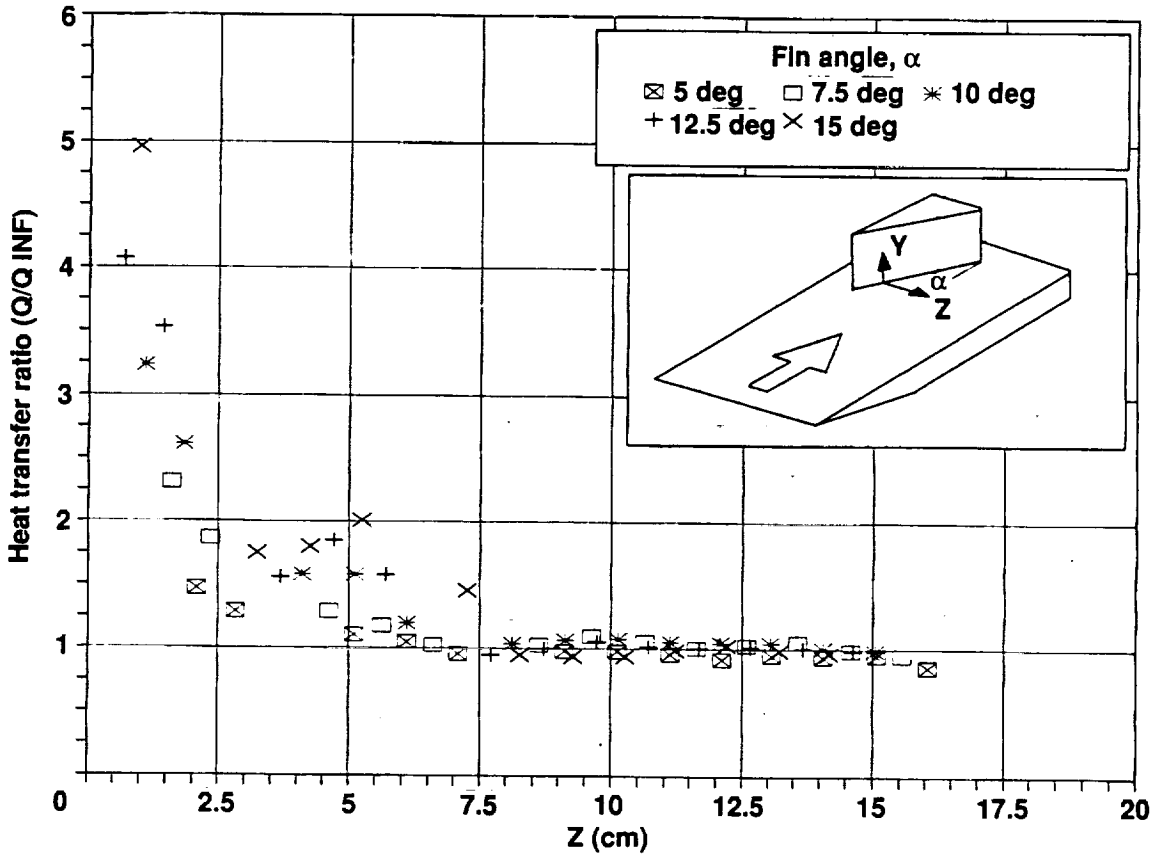

Figure 11. Heat transfer distribution on flat plate surface.

NASA
National Aeronautics and Space Administration

Report Documentation Page

1. Report No.	2. Government Accession No.	3. Recipient's Catalog No.
NASA TM-103838		

4. Title and Subtitle

Documentation of Two- and Three-Dimensional Shock-Wave/ Turbulent-Boundary-Layer Interaction Flows at Mach 8.2

5. Report Date

May 1991

6. Performing Organization Code

7. Author(s)

M. I. Kussoy* and K. C. Horstman*

8. Performing Organization Report No.

A-91069

10. Work Unit No.

505-59-40

9. Performing Organization Name and Address

Ames Research Center
Moffett Field, CA 94035-1000

11. Contract or Grant No.

13. Type of Report and Period Covered

Technical Memorandum

12. Sponsoring Agency Name and Address

National Aeronautics and Space Administration
Washington, DC 20546-0001

14. Sponsoring Agency Code

15. Supplementary Notes

Point of Contact: C. C. Horstman, Ames Research Center, MS 229-1, Moffett Field, CA 94035-1000
(415) 604-6255 or FTS 464-6255

*Eloret Institute, 3788 Fabian Way, Palo Alto, CA 94303

16. Abstract

Experimental data for a series of two-dimensional and three-dimensional shock-wave/turbulent-boundary-layer interaction flows at Mach 8.2 are presented. The test bodies, composed of simple geometric shapes fastened to a flat plate test bed, were designed to generate flows with varying degrees of pressure gradient, boundary-layer separation, and turning angle. The data include surface pressure and heat transfer distributions as well as limited mean flow field surveys both in the undisturbed and interaction regimes. The data are presented in a convenient form to be used to validate existing or future computational models of these hypersonic flows. Additional data are on a computer disk included with this document. This work was supported by a grant from NASA to Eloret Institute (NCC2-452).

17. Key Words (Suggested by Author(s))	18. Distribution Statement
Hypersonic Boundary layer Shock wave	Unclassified-Unlimited Subject Category - 34

19. Security Classif. (of this report)	20. Security Classif. (of this page)	21. No. of Pages	22. Price
Unclassified	Unclassified	46	A03